Environmental Fluid Mechanics **4:** 273–303, 2004.

Simulation of Ekman Boundary Layers by Large Eddy Model with Dynamic Mixed Subfilter Closure

I. ESAU
Department of Earth Science, Meteorology, Uppsala University, Sweden, currently at NERSC, Bergen, Norway

Received 9 December 2002; accepted in revised form 5 January 2004

Abstract. Theoretical analysis of boundary layer turbulence has suggested a feasibility of sufficiently accurate turbulence resolving simulations at relatively coarse meshes. However, large eddy simulation (LES) codes, which employ traditional eddy-viscosity turbulence closures, fail to provide adequate turbulence statistics at coarse meshes especially within a surface layer. Manual tuning of parameters in these turbulence closures may correct low order turbulence statistics but severely harms spectra of turbulence kinetic energy (TKE). For more than decade, engineering LES codes successfully employ dynamic turbulence closures. A dynamic Smagorinsky turbulence closure (DSM) has been already tried in environmental LES. The DSM is able to provide adequate turbulence statistics at coarse meshes but it is not completely consistent with the LES equations. This paper investigates applicability of an advanced dynamic mixed turbulence closure (DMM) to simulations of Ekman boundary layers of high Reynolds number flows. The DMM differs from the DSM by explicit calculation of the Leonard term in the turbulence stress tensor. The Horizontal Array Turbulence Study (HATS) field program has revealed that the Leonard term is indeed an important component of the real turbulence stress tensor.

This paper presents validation of a new LES code LESNIC. The study shows that the LES code with the DMM provides rather accurate low order turbulence statistics and the TKE spectra at very coarse meshes. These coarse LES maintain more energetic small scale fluctuations of velocity especially within the surface layer. This is critically important for success of simulations. Accurate representation of higher order turbulence statistics, however, requires essentially better LES resolution. The study also shows that LES of the Ekman boundary layer cannot be directly compared with conventionally neutral atmospheric boundary layers. The depth of the boundary layer is an important scaling parameter for turbulence statistics.

Key words: Large eddy simulation, planetary boundary layers, turbulence

Abbreviations: LES – Large eddy simulation; PBL – Planetary boundary layer; DMM – Dynamic mixed subfilter closure; DSM – Dynamic Smagorinsky subfilter closure; TSM – Traditional Smagorinsky subfilter closure; TKE – Turbulent kinetic energy; LQ79 – Leslie and Quarini [27]; Re – Thickness Reynolds number.

*Corresponding address: Nansen Environmental and Remote Sensing Centre, Edvard Griegsvei 3A, 5059 Bergen, Norway, E-mail: igore@nersc.no

1. Introduction

Large eddy simulation technique (LES) is gradually becoming a common tool in research studies of planetary boundary layers (PBLs). There are three main direction of the LES development [1].

Following the first direction, authors try to resolve as small as possible turbulent scales in PBLs. The kinetic energy of turbulent fluctuations (TKE) at the small scales comprises only a small part of the total TKE. Therefore, even large errors in calculations of the small scales have a negligible effect on quality of simulations. This advantage makes fine scale LES runs robust and independent of the employed turbulence closure. However, the price of quite modest improvements seems to be too high [2].

Following the second direction, authors try to apply results from the low Reynolds number (Re) direct numerical simulations or results from the low dimensional modeling to high Re PBLs. Such attempts must be considered with a great caution [3] since the nature of the high Re PBL turbulence seems to be essentially different from the nature of the low Re laboratory turbulence [4, 5].

The third direction is followed in this paper. Briefly, this direction can be characterized as 'improvement of turbulence closures'. Physically, this improvement is possible due to universal nature of the small scale turbulence. This universality has found its mathematical expression in the Kolmogorov's law for the inertial interval of scales. According to Kolmogorov [6], the TKE of the tree-dimensional turbulence is $E(k) = C_K \varepsilon^{2/3} k^{-5/3}$, where C_K is the Kolmogorov's constant, ε is energy dissipation and k is a wave number. At high Re, the energy dissipation, ε, is independent of k. The existence of the wide inertial interval of scales is confirmed by a number of measurements both in laboratory experiments (e.g., [7]) and field campaigns (e.g., [8]).

The Kolmogorov's law is extremely useful for construction of turbulence closures. For instance, it is easy to relate the TKE at some resolved wave number, k_r, with the TKE at subgrid wave numbers, $k > k_c$, where k_c is the model cut-off wave number. The expression is $E(k_r)/E(k > k_c) = 2/3(k_c/k_r^{5/2})^{2/3}$. This idea was used for construction of a structure-function turbulence closure by Chollet and Lesieur [9] (in Fourier space) and Metais and Lesieur [10] (in physical space).

Piomelli [11] noticed that the structure-function turbulence closure cannot follow actual turbulence spectra, which may significantly deviate from the Kolmogorov's law at large scales. Dynamic turbulence closures (DTCs) are more general and more flexible. Germano's identity [12], see Section 2.2, one essential component of the DTCs, is true for any spectral intervals. However, another essential component of the DTCs, the Smagorinsky–Lilly relation for the eddy viscosity, $K_m = (C_s \Delta)^2 |S_{ij}|$ [13], is true only for steady state homogeneous and isotropic turbulence, i.e., only for turbulence in the inertial interval of scales [14]. The DTCs try to minimize the discrepancy resulting from application of the Smagorinsky–Lilly relation to the actual turbulence in simulations.

The actual turbulence in LES may or may not be resolved down to the inertial interval of scales. If LES do resolve a part of the inertial interval then the DTCs simply reproduce the Kolmogorov's law. However, LES of PBLs always have some layers, one close to the surface and others with strong stable stratification, where the inertial interval of scales is unresolved. Those layers are important to have a success in simulations of the whole PBL.

Variety of possible optimization approaches and additional physical assumptions determine a great number of proposed dynamic turbulent closures [11]. The simplest of them like the dynamic Smagorinsky closure (DSM) by Germano *et al.* [12] and the dynamic mixed closure (DMM) by Zang *et al.* [15] optimize only one parameter, namely, the constant C_s.

It is always desirable to achieve more realistic LES with less sophisticated turbulence closures using a relatively coarse grid. Moreover, practical micrometeorological simulations should resolve local circulation systems and turbulence depending physical processes. Nowadays such simulations are possible in PBLs at resolution larger than about 100 m. Chapman [7] and more recently Baggett *et al.* [16] examined resolution requirements for boundary layer flows. Chapman analytically estimated that $C_f \mathrm{Re}^{0.4}$ grid points in a volume H^3 are sufficient to resolve a given fraction of the TKE in boundary layer flows. Here, H is the boundary layer thickness and C_f is a proportionality constant. This constant determines the resolved fraction of the TKE. Given the large scatter in the PBL data, this estimation suggests that an ideal LES code will provide reliable turbulent statistics using only 10 to 20 grid points on the length scale H. Consistently, Baggett *et al.* [16] concluded on the basis of an independent study that an 'engineering' resolution requirement is about 10 grid points on the length scale H. Both analysis suggest a possibility of very coarse resolution LES with grid scales 50–150 m in atmospheric PBLs.

Published LES (e.g., [17–21]) provide some credit to the theoretical estimations. However, they also demonstrate that robustness of the coarse resolution LES greatly depends on employed turbulence closures. As the matter of fact, the turbulence closures which explicitly account for the flow anisotropy have demonstrated better representation of the PBL turbulence [18, 22, 23]. The DSM and DMM account for the flow anisotropy locally and instantly. It suggests that their implementation will further improve coarse resolution simulations of PBLs. Moreover, the DMM is attractive since it naturally follows from the filtered Euler equations for incompressible fluid.

The DMM has demonstrated excellent performance in different engineering applications (e.g. [15, 24, 25]). In spite of this fact, Mason [19] casted doubt on applicability of dynamic turbulence closures to PBL simulations. One of Mason's arguments ([19], p. 17) was that the DTCs allow for a systematic enhancement of resolved velocity gradients, ∇u_i^l. The systematic enhancement does not agree with predictions of spectral theories [26], [27], hereafter LQ79. The spectral theories

suggest that such an enhancement should not result from stochastic forcing with random phases.

As the matter of fact, the stochastic forcing appears due to neglecting of the statistical correlations between the motions on different scales ([26], p. 1522). This is consistent with the Kolmogorov's law but inconsistent with the actual dynamics of incompressible fluid. Incompressible fluid cannot have uncorrelated motion on smallest resolved and largest unresolved scales without violation of continuity. The scale-similarity part in the DMM accounts for these statistical correlations. These statistical correlations are rather small in high Re flows. Tong *et al.* [28] obtained the correlations 0.07–0.09 from measurements in a weakly unstable PBL. It may explain a success of a stochastic turbulence closure proposed by Mason and Thomson [22].

The systematic enhancement of ∇u_i^l also stands against the systematic smoothing of ∇u_i^l by numerical schemes [29]. The systematic smoothing of ∇u_i^l determines relatively low Re_λ of LES simulations [30], where Re_λ is the Reynolds number based on the Taylor microscale. In turn, low Re_λ of actual LES give rise to larger correlations than it can be observed in real PBLs.

This study is not the first attempt to utilize the dynamic turbulence closures in PBL simulations. Up to the author's knowledge, there were just two attempts to use LES with the DSM in environmental studies. Porte-Agel *et al.* [21] have applied such LES to study an atmospheric boundary layer without an action of the Coriolis force. Zikanov *et al.* [31] and Zikanov *et al.* [32] have applied such LES to study the oceanic mixing and the oceanic Ekman boundary layers respectively.

This paper presents a finite-difference LES code with the DMM (Section 2). The code, nicknamed LESNIC, was developed by the author at the Department of Earth Sciences, Uppsala University. This study addresses different issues related to the implementation of the DMM (Section 2.2). The DMM is not only more natural choice than the DSM but it also provides more accurate representation of PBL turbulence. The latter clearly follows from Sullivan *et al.* [33] study of data, which has been obtained during the Horizontal Array Turbulence Study field program. The study is mainly aimed to demonstrate a potentially high quality of LES at coarse resolution grids (Section 3). It investigates effects of the LES resolution and the turbulence closures on the turbulent statistics in PBLs attempting to find limits of the LES applicability. Section 4 outlines conclusions of this study. Appendix A describes set up of the numerical experiments.

2. Large Eddy Simulation Technique

2.1. EQUATIONS

The high Re number LES technique is essentially based on the convolution of the Euler equations with some low-pass filter. The resulting large scale Euler equations for incompressible Boussinesq's fluid read

$$\frac{\partial u_i^l}{\partial t} = -\frac{\partial}{\partial x_j}(u_i^l u_j^l + \tau_{ij} + p^l \delta_{ij}) - f\omega_j \delta_{ij} - g\beta\Theta^l \delta_{i3}, \tag{1}$$

$$\frac{\partial u_i^l}{\partial x_i} = 0, \tag{2}$$

$$\frac{\partial \Theta^l}{\partial t} = -\frac{\partial}{\partial x_j}(\Theta^l u_j^l + \tau_{\Theta j}). \tag{3}$$

Everywhere in this paper, the superscript l denotes filtered (resolved) variables, the superscript L denotes variables filtered with a wider filter

$$u_i^l = \int_a^b u_i(x_j')G_\Delta(x_j - x_j')dx_j', \quad u_i^L = \int_a^b u_i(x_j')G_{\alpha\Delta}(x_j - x_j')dx_j', \tag{4}$$

$$a = x_j - \Delta_j/2, \qquad b = x_j + \Delta_j/2.$$

The superscript s denotes subfilter variables $u_i^s = u_i - u_i^l$. Here $x_j = (x, y, z)$ are the axes of the Cartesian coordinate system directed to East, North and Zenith, $u_i = (u, v, w)$ are the velocity components and $\Delta_j = (\Delta_x, \Delta_y, \Delta_z)$ are the grid scales. The filtered potential temperature Θ^l[1] and the filtered dynamic pressure p^l are defined in the same way. The filter function, $G_{\alpha\Delta}(x_j - x_j')$, is used only to calculate the subfilter turbulent stress, τ_{ij}, and the subfilter temperature diffusion, $\tau_{\Theta j}$. The following Gaussian filter is used

$$G_{\alpha\Delta}(x_j - x_j') = \sqrt{\frac{6}{\pi(\alpha\Delta_j)^2}} \exp\left(-\frac{6(x_j - x_j')^2}{(\alpha\Delta_j)^2}\right). \tag{5}$$

The filter works successively in x and y directions. Variables remain unfiltered in the inhomogeneous, z, direction as it has been argued by Ghosal *et al.* [34].

The vertical and the horizontal components of the Earth rotation are taken into account through the Coriolis parameter, $f = 2\Omega \sin\varphi$, where $\Omega = 7.45 \cdot 10^{-5}$ s^{-1} is the constant angular velocity and φ is a latitude. The components of the Coriolis force are $f\omega_j = f\{(u_2^g - u_2^l - u_3^l ctg\varphi), (-u_1^g + u_1^l), u_1^l ctg\varphi\}$. At the middle and high latitudes, the mean pressure gradient relates to the geostrophic wind as $u_i^g =$

[1] Only $\partial\Theta^l/\partial z$ affects fluid motions therefore, in order to keep numerical errors small, initial values of Θ^l are always chosen as small as possible.

$1/f \cdot (-\partial P/\partial y, \partial P/\partial x, 0)$. The thermal expansion coefficient is $\beta = 0.003$ K^{-1}, $g = 9.81$ m s^{-2} is the acceleration due to gravity.

The Einstein's notation is used for summation. In this notation, $\delta_{ij} = 1$ at $i = j$ and $\delta_{ij} = 0$ at $i \neq j$.

2.2. SUBFILTER (SUBGRID) TURBULENT CLOSURE

Terms τ_{ij} and $\tau_{\Theta j}$ in Equations (1) and (3) include unknown subfilter variables. They must be expressed in terms of the filtered variables only. Some physical assumptions have to be done to obtain the explicit expressions for τ_{ij} and $\tau_{\Theta j}$.

Germano [35] discussed the exact form of the subfilter stress in Equation (1),

$$\tau_{ij}(u_i, u_j) = (u_i u_j)^l - (u_i)^l (u_i)^l. \tag{6}$$

Define decomposition of the velocity on the resolved and unresolved parts as $u_i = u_i^l + u_i^s$. Substitution of this decomposition into Equation (6) gives

$$\tau_{ij}(u_i, u_j) = L_{ij} + C_{ij} + R_{ij}, \tag{7}$$

where

$$L_{ij} = (u_i^l u_j^l)^l - (u_i^l)^l (u_i^l)^l \tag{8}$$

is the Leonard term,

$$C_{ij} = (u_i^s u_j^l)^l - (u_i^s)^l (u_i^l)^l + (u_i^l u_j^s)^l - (u_i^l)^l (u_i^s)^l \tag{9}$$

is the Cross term and

$$R_{ij} = (u_i^s u_j^s)^l - (u_i^s)^l (u_i^s)^l \tag{10}$$

is the Reynolds term. This definition of the subfilter stress tensor recovers the Galilean invariance of Equation (1).

Two-dimensional filtration assigns the following physical meaning to these terms. The Reynolds term, R_{ij}, is responsible for the energy dissipation. The Cross term, C_{ij}, is responsible for the energy backscatter from small scales to large scales. LQ79 found that $|C_{ij}|$ can be as large as $|R_{ij}|$.

In the case of the two-dimensional filtration, the net energy dissipation is a small difference between large terms R_{ij} and C_{ij}. This is not true in the cases of one- and three-dimensional filtrations. Figure 1 shows these three terms in τ_{13} component of the subfilter stress in the PBL128-DMM run (see the run description in Appendix A). Here, u_i^L is used instead of u_i^l and $u_i^s = (u_i^l - u_i^L)$ is used instead of unknown u_i^s. A striking property of this Figure is an anti-correlation between C_{ij} and other terms in the turbulent stress decomposition. This anti-correlation contradicts Sullivan *et al.* [33] analysis of the HATS data. It also contradicts Salvetti and Banerjee [36] and Salvetti and Beux [37] analysis of LES data. These works suggests that all components of τ_{ij} must be positively correlated. This controversy is caused by the difference in the dimension of the filter kernel. The mentioned

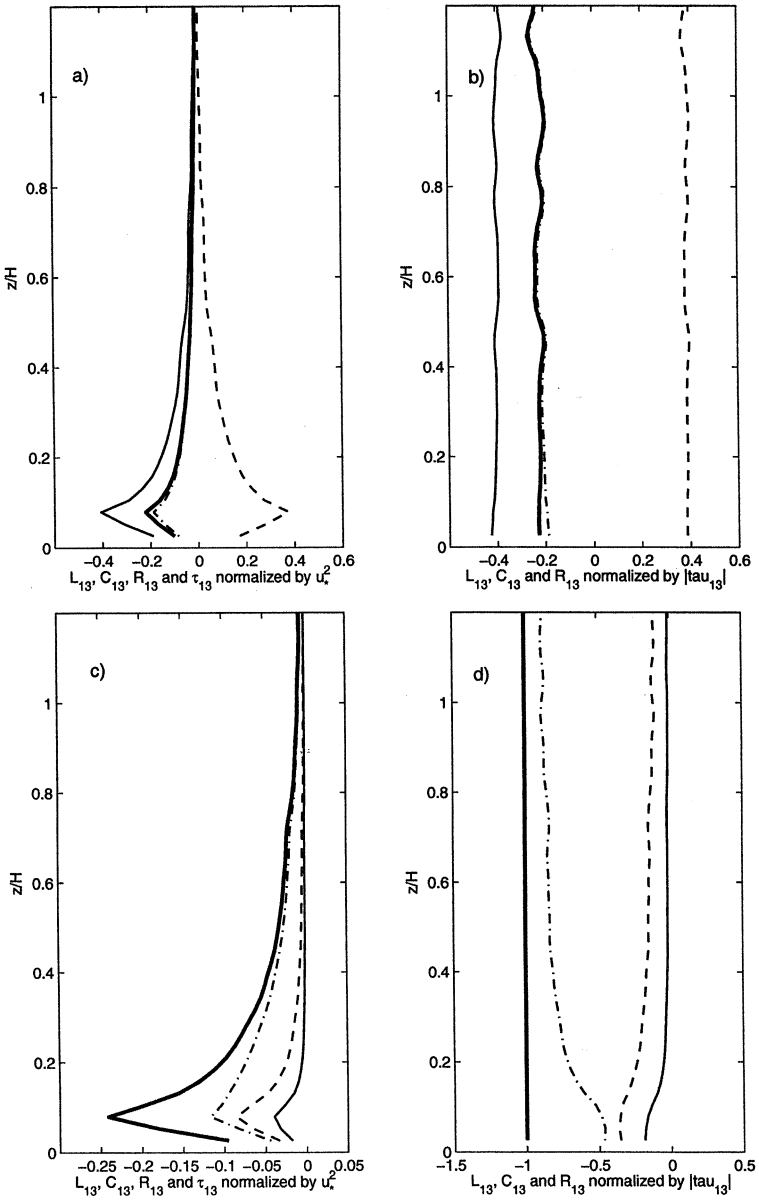

Figure 1. Profiles of the Reynolds, R_{13} (solid line), the Cross, C_{13} (dashed line), and the Leonard, L_{13} (dash-dotted line), terms of τ_{13} (bold solid line) component of the subfilter stress from the run PBL128-DMM. Substitutions $u_i^l = u_i^L$ and $u_i^s = (u_i^l - u_i^L)$ are used to calculate these profiles. Panels (a) and (b) present the terms resulting from two-dimensional filtration, which is actually implemented in LESNIC. Panels (c) and (d) present the terms resulting from three-dimensional filtration, which is consistent with Sullivan *et al.* [33] procedure. All terms are normalized by the surface stress velocity, u_*^2 (a), and the absolute turbulent stress, $|\tau_{13}| = (L_{13}^2 + C_{13}^2 + R_{13}^2)^{1/2}$ (b).

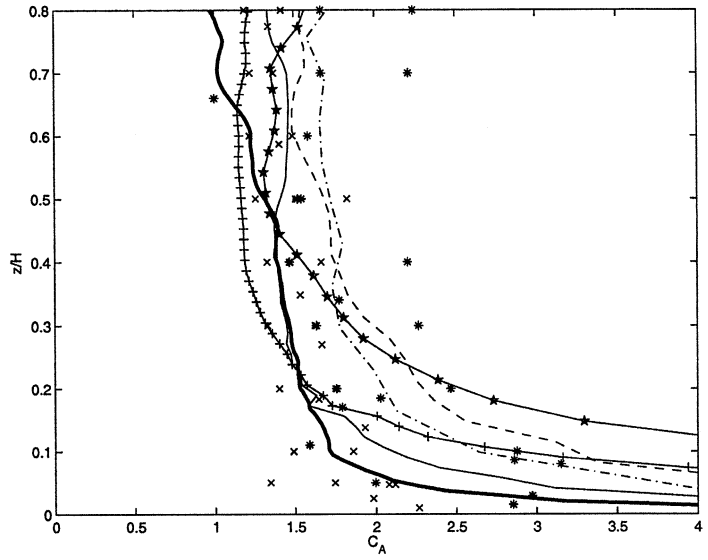

Figure 2. Profiles of the anisotropy coefficient, $C_A = 2E/3\sigma_{ww}^2$ in neutral boundary layers: — run PBL128-DMM; — run PBL64-DMM; – – – run PBL32-DMM; – · – run PBL16-DMM; –⋆– run PBL32-TSM1; –+– run PBL64-TSM1. Symbols are: × – laboratory data from [38] and [39]; ∗ – atmospheric data from [40], [41] and [42].

works rely on three-dimensional filtration. Application of three-dimensional filter in the present LES code (see Figures 1c,d) recovers positive correlations of all terms in τ_{ij}. However, three-dimensional filtration is mathematically inconsistent

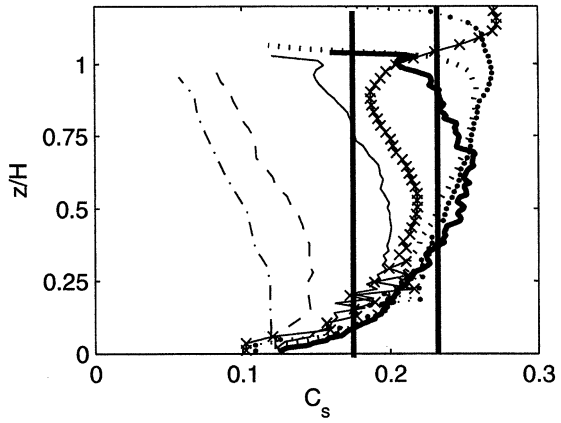

Figure 3. Profiles of the Smagorinsky constant, C_s in LES with the DMM: — run PBL128-DMM; — run PBL64-DMM; – – – run PBL32-DMM; – · – run PBL16-DMM; · · · · · · · run PBL80-DMM; · · ● · · ● · · run PBL64-DMM-H500; –×– run PBL64-DMM-CI. The straight lines embrace the theoretical estimations, $0.176 < C_s < 0.23$, from [27] and [13].

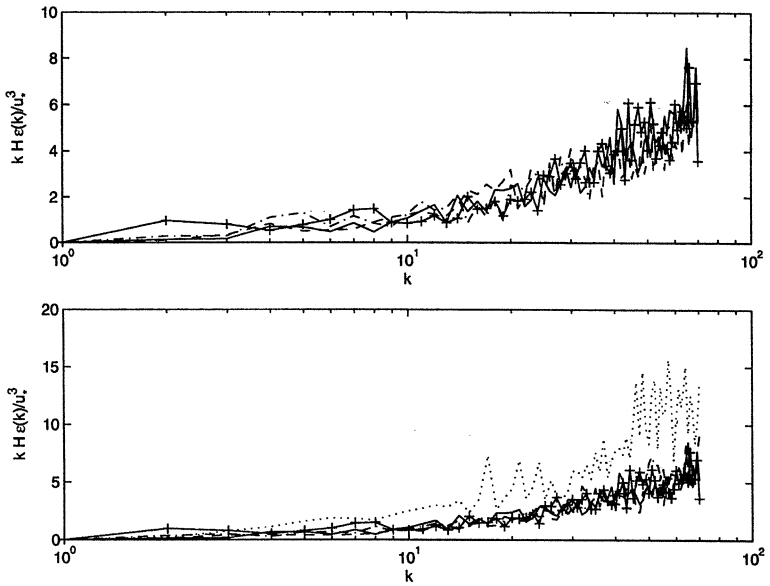

Figure 4. Time spectra of normalized energy dissipation, $kH\varepsilon/u_*^3$, where k is number of 10 min. cycles. The upper panel presents the spectra at different resolutions: — run PBL64-DMM; – – – run PBL32-DMM; – · – run PBL16-DMM;– + – run PBL64-DMM-CI. The lower panel presents the spectra from LES with different turbulence closures: — run PBL64-DMM; – – – run PBL64-DSM; – · – run PBL64-TSM0; · · · · · · · run PBL64-TSM1.

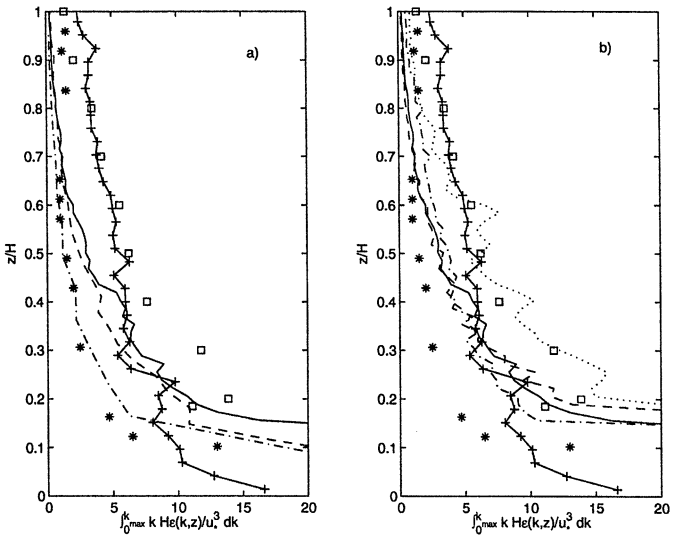

Figure 5. Profiles of normalized energy dissipation, $\int_0^{k_{max}} kH\varepsilon(k,z)/u_*^3 dk$, from LES at different resolutions (a): — run PBL64-DMM; – – – run PBL32-DMM; – · – run PBL16-DMM;– + – run PBL64-DMM-CI; and from LES with different turbulence closures (b): — run PBL64-DMM; – – – run PBL64-DSM; – · – run PBL64-TSM0;· · ·· run PBL64-TSM1; – + – run PBL64-DMM-CI. Symbols are PBL data: ∗ from [43]; □ from [40].

with boundary layer turbulence and may amplify large numerical errors at the surface proximity [34].

Turbulent closures accounting for the Reynolds term only are overdissipative (e.g., [17, 19, 22]). They dissipate about twice as much energy as it really occurs in the flow (Figure 1b). This fact explains why the Smagorinsky constant, $C_s = 0.1$, suits boundary layer simulations much better than the analytically derived $C_s \in [0.17; 0.23]$. The Leonard term, L_{ij}, used to be neglected even in backscatter subfilter closures [22]. However, it was recognized that L_{ij} is responsible for up to 14% of the total energy transfer in the LES with the Gaussian or the top-hat filters (LQ79, see also Figure 1b).

To construct a practically usable turbulence closure, we employ the Smagorinsky–Lilly eddy-viscosity assumption [13, 14]

$$K_m = l_s^2 |S_{ij}^l|, \tag{11}$$

where the velocity strain rate tensor is

$$S_{ij} = \frac{1}{2}\left(\frac{\partial u_i}{\partial x_j} + \frac{\partial u_j}{\partial x_i}\right). \tag{12}$$

Physically, this assumption means that the simulated turbulence at scales Δ and $\alpha\Delta$ is within the inertial interval of scales. Clearly, this is not the case with coarse resolution LES. Application of (11) to virtually any type of flows will give rise to an error. The error can be minimized considering the dissipative length scale, l_s, as a free parameter. The Smagorinsky–Lilly assumption also justifies the use of

$$L_{ij}^L = (u_i^l u_j^l)^L - (u_i^l)^L (u_j^l)^L \tag{13}$$

instead of L_{ij} in Equation (8) [44]. The tensor L_{ij}^L constitutes the scale-similarity part of the DMM. It works reasonably well in strongly anisotropic flows, where correlations between large- and small-scale fluctuations are significant. However, it does not dissipate enough energy in almost isotropic flows, where such correlations are rather small. Figure 2 shows the anisotropy profiles of velocity fluctuations in PBLs (see the run descriptions in Appendix A).

The DMM parameterizes the sum $C_{ij} + R_{ij}$ in (8) using the eddy-viscosity assumption as

$$C_{ij} + R_{ij} = -2K_m S_{ij}^l = -2l_s^2 |S_{ij}^l| S_{ij}^l, \tag{14}$$

The weight of the eddy-viscosity part given by Equation (14) in the DMM must decrease with increasing of the flow anisotropy.

Traditionally, the dissipation length scale, l_s, is related to the grid scale Δ as $l_s = C_s\Delta$ [13], where C_s is the Smagorinsky constant. Considering C_s as the true physical constant, Sullivan *et al.* [23] proposed to change the definition of the velocity strain rate, S_{ij}^l, to recover the decrease of the eddy viscosity in anisotropic flows. On the contrary, the DMM considers S_{ij}^l as a physically meaningful

quantity. The dissipation length scale l_s, which has physically unclear meaning, is considered as a free parameter for optimization.

Finally, the DMM in Vreman *et al.* [24] formulation reads

$$\tau_{ij}^* = \underbrace{(u_i^l u_j^l)^L - (u_i^l)^L (u_j^l)^L}_{\text{scale similarity part}} - \underbrace{2l_s^2 |S_{ij}^l| S_{ij}^l}_{\text{eddy viscosity part}} . \tag{15}$$

The resolved tensor τ_{ij}^* approximates the exact subfilter stress tensor, τ_{ij}, with some error ϵ_{ij}. This error can be minimized by an appropriate choice of l_s at every grid point and at every time step. The dynamic approach employs the Germano's identity and the least square minimization method to recover the most optimal values of l_s. The Germano's identity gives

$$H_{ij}^L - L_{ij}^L + 2l_s^2 M_{ij}^L = \epsilon_{ij}, \tag{16}$$

where

$$M_{ij}^L = (|S_{ij}^l| S_{ij}^l)^L - \alpha^2 |(S_{ij}^l)^L| (S_{ij}^l)^L, \tag{17}$$

$$\begin{aligned} H_{ij}^L = & \left(\left((u_i^l)^L (u_j^l)^L \right)^l \right)^L - \left(\left((u_i^l)^L \right)^l \right)^L \left(\left((u_j^l)^L \right)^l \right)^L - \\ & \left(\left((u_i^l)^l \right)^L \left((u_j^l)^l \right)^L - \left((u_i^l)^l (u_j^l)^l \right)^L \right). \end{aligned} \tag{18}$$

Vreman *et al.* [25] analytically found $\alpha^2 = 5^{2/3} \approx 2.92$ for the Gaussian and the top-hat filters with the filter width ratio $\Delta_x^L / \Delta_x^l = \Delta_y^L / \Delta_y^l = 2$, $\Delta_z^L / \Delta_z^l = 1$.

Let us define the scalar product of two tensors A_{ij} and B_{ij} with components a_{ij} and b_{ij}, $i, j = 1, 2, 3$, as $A_{ij} \cdot B_{ij} = \sum_{i,j} a_{ij} b_{ij}$ and the energetic norm of the tensor A_{ij} as $||A_{ij}||_2 = (A_{ij} \cdot A_{ij})^{1/2}$. The least square minimization method applied to Eq. (16) gives

$$\frac{\partial ||\epsilon_{ij}||_2^2}{\partial l_s^2} = 4(H_{ij}^L - L_{ij}^L) \cdot M_{ij}^L + 8l_s^2 ||M_{ij}^L||_2^2 = 0. \tag{19}$$

The above equation gives the final expression for the free parameter

$$l_s^2 = \frac{1}{2} \frac{(L_{ij}^L - H_{ij}^L) \cdot M_{ij}^L}{||M_{ij}^L||_2^2}, \tag{20}$$

The computation of l_s is heavily sensitive to the smallest resolved motions. Therefore, it is a mathematically ill-posed problem. To stabilize computations, it was prescribed that $-0.01 \le l_s/\Delta \le 0.8$. This is not too restrictive. The average value of $l_s/\Delta \in [0.18; 0.23]$. Figure 3 shows typical non-dimensional profiles of l_s/Δ in PBLs provided by LES with the DMM at different resolutions. The filter scale $\Delta = (\Delta_x \Delta_y \Delta_z)^{1/3}$ is a constant here. A strong reduction of the dissipative length scale is obvious within a surface layer as well as in a stably stratified inversion layer.

The turbulent diffusion of potential temperature is parameterized in the following way

$$\tau_{\Theta j} = -\mathrm{Pr}_{LES}^{-1} l_s^2 |S_{ij}^l| \frac{\partial \Theta^l}{\partial x_j}, \tag{21}$$

where Pr_{LES} is a subgrid Prandtl number. Kondo *et al.* [45] proposed an empirical relation

$$\mathrm{Pr}_{LES}^{-1} = \begin{cases} \frac{1}{7Ri_g}, & 1 \le Ri_g, \\ \frac{1}{6.873 Ri_g + \frac{1}{1+6.873 Ri_g}}, & 0.01 < Ri_g \le 1 \\ 1.5, & Ri_g \le 0.01, \end{cases} \tag{22}$$

where $Ri_g = g\beta \nabla_z \Theta / \left((\nabla_z u)^2 + (\nabla_z v)^2 \right)$ is the gradient Richardson number.

2.3. NUMERICAL IMPLEMENTATION

This LES code is a finite difference code of the second order of accuracy. The code employs a fully conservative central difference scheme [46] with the non-linear advection discretized in a skew-symmetric form. All variables are discretized on the staggered C-type grid with the pressure and the potential temperature at centers of cells.

Although the scheme is not monotonous, no limiter is applied to correct the simulations. Non-monotonous schemes give rise to numerical ripples around any physical fluctuation of the velocity or temperature. Amplitudes of the ripples are proportional to the gradients of variables. The turbulence closure effectively damps these numerical ripples since the eddy viscosity and diffusivity are also proportional to the gradients. Problems may appear only in simulations of very stable PBLs, where the turbulent dissipation and diffusion are naturally small. Nevertheless, the amplitudes remain negligible if physical fluctuations exist relatively small number (about 100) of time steps.

Sagaut and Grohens [47] showed that optimal discrete forms of the Gaussian and the top-hat (grid) filters coincide for central difference schemes of the second order of accuracy. It makes the LES code of the second order of accuracy self-consistent. The discrete compact filter in e.g., x direction reads

$$u_i^l(X) = a\ (u_i(X + \Delta_x) + u_i(X - \Delta_x) + b\ u_i(X)), \tag{23}$$

where $u_i(X)$ is the velocity at the grid point X. The coefficients a, b are equal to 1/24 and 22 for the basic filter G_Δ, and 1/6 and 4 for the wider filter $G_{\alpha\Delta}$.

The Equations (1) and (3) are integrated in time using Runge–Kutta scheme in Jameson *et al.* [48] formulation. The time step is variable. It can be estimated (B-J. Boersma, personal communication) as

$$\Delta_t = C_{CFL} \left(\frac{u_i^l}{\Delta_{x_i}} + l_s^2 |S_{ij}^l| \left(\frac{1}{\Delta_x^2} + \frac{1}{\Delta_y^2} + \frac{1}{\Delta_z^2} \right) \right)^{-1}. \tag{24}$$

Here, C_{CFL} is the Courant number. The fourth order Runge–Kutta scheme allows $C_{CFL} = 2.89$. The large Courant number makes this LES code about 4–5 times more computationally efficient than a traditional LES code with the leapfrog or Adams–Bashforth schemes.

Incompressibility is enforced by velocity correction through dynamic pressure calculation. The dynamic pressure is calculated by means of a fractional step method by Kim and Moin [49] with modifications by Armfield and Street [50]. In this set of methods, the corrected velocity is not an exact discrete solution of the Euler equations. To satisfy both the continuity and the Euler equations, the velocity field must be iterated several times at every time step. This LES code does not use iterations since the improvement is rather small.

Non-slip boundary conditions cannot be employed in the LES code. Firstly, they are not physical for large resolved eddies. Large eddies like, for example, tornado or thermals can slip over the surface. Secondly, high Re flows develop the logarithmic mean velocity profile in the surface layer. This profile has a strong curvature in the surface proximity. Strongly curved profiles cannot be correctly approximated by finite difference schemes. A direct implementation of the Dirichlet conditions $u_i(z = 0) = 0$ would result in a thick viscous sublayer. As in majority of LES codes [17], this LES code employs the logarithmic law (log-law) to match the high Re surface conditions. The 2nd order central difference scheme along with the C-type staggered grid require only tangential subfilter stresses, τ_{i3} and $\tau_{\Theta 3}$, to be defined at the non-slip boundary. For simplicity, the influence of pressure gradients, buoyancy and non-linear accelerations are neglected below the first grid level. It gives $|\tau_{k3}| = u_*^2$, $k = 1, 2$ at the surface. The surface stress velocity, u_*, can be determined from the log-law for a rough surface and the velocity at the first computational level $\Delta_z/2$ as

$$u_* = \frac{1}{\frac{1}{\kappa}\ln\left(\frac{\Delta_z}{2z_0}\right)}|u_i(x, y, \Delta_z/2)|, \tag{25}$$

where z_0 is surface roughness and $\kappa = 0.41$ is the von Karman constant. Finally, the subfilter surface stress reads

$$\tau_{k3}(z = 0) = u_*^2 \frac{u_k(x, y, \Delta_z/2)}{|u_k(x, y, \Delta_z/2)|}, \quad k = 1, 2. \tag{26}$$

The subfilter surface heat flux, $\tau_{\Theta 3}$, is prescribed explicitly. Von Neumann boundary conditions set up at the upper boundary

$$\frac{\partial u_k(x, y, z = L_3)}{\partial z} = \frac{\partial \Theta(x, y, z = L_3)}{\partial z} = 0, \quad k = 1, 2. \tag{27}$$

The Dirichlet condition must be used for the vertical component of velocity, $w(x, y, z = L_3) = 0$.

Lateral boundary conditions are periodic in this LES code.

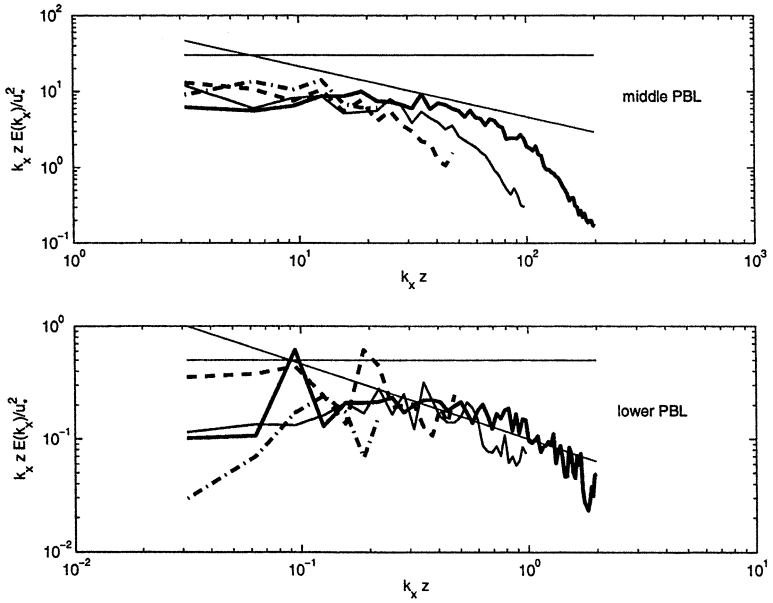

Figure 6. Non-dimensional streamwise spectra of the TKE, $k_x z E(k_x)/u_*^2$, in the middle $0.3H - 0.7H$ and lower $0H - 0.15H$ parts of the PBL: — run PBL128-DMM; — run PBL64-DMM; – – – run PBL32-DMM; – · – run PBL16-DMM. The straight lines shows the theoretical spectral slopes in the inertial interval of scales $(k_x) \cdot k_x^{-5/3}$ and in the energy production interval of scales $(k_x) \cdot k_x^{-1}$

3. Quality of Large Eddy Simulations

3.1. CONCEPT OF LES FLUID

Two physically different fluids are called similar if they have equal non-dimensional numbers. These numbers follow from a proper normalization of the equations describing the behavior of fluids. The LES equation (1) does not possesses the important Re number characterizing the dissipation in Newtonian fluids. In fact, the LES equations describe hypothetical non-Newtonian fluid. Muschinski [30] called it 'LES fluid'.

Strictly speaking, LES fluid is not similar to any of environmental fluids with small but linear viscosity. Thus, direct comparison of LES and experimental statistics is not justified. At the same time, one of the main features of three-dimensional isotropic turbulence is that at high Re, the rate of energy dissipation, ε, is independent of the structure of viscosity ([51], p. 179). Hence, the fundamental parameter making LES and environmental fluids similar is the rate of energy dissipation. The spectra of the TKE dissipation are shown in Figure 4. Indeed, they demonstrate a remarkable collapse to each other except for the dissipation in LES with the TSM1. This closure is known to be overdissipative. The collapse gives some credit to our

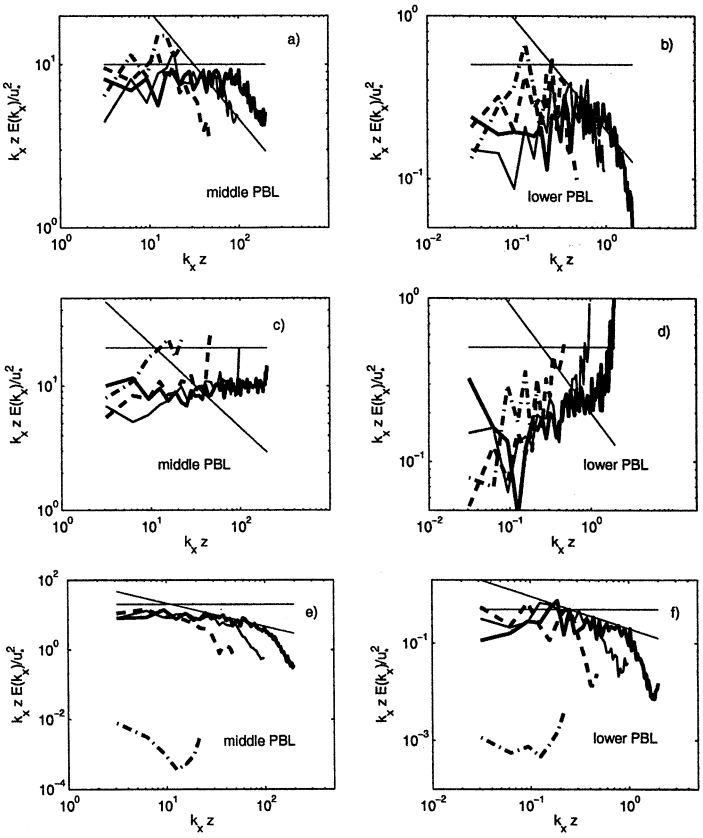

Figure 7. The same as in Fig. 6 but for LES with the DSM, panels (a) and (b), with the TSM0 $C_S = 0.06$, panels (c) and (d), and with the TSM1 $C_S = 0.23$, panels (e) and (f).

view of the dissipation as a key characteristic of the high Re LES. Figure 5 shows that all LES runs have the dissipation within the scatter of PBL data.

It is possible to construct a non-dimensional number equally suitable for identifications of dynamical stability in both Newtonian and non-Newtonian fluids. This non-dimensional number should not refer to the molecular viscosity as a material property of fluid. The LES fluid does not possess such a material property. Instead, it should refer to the vorticity structure and the dissipation length scale in fluid. One of suitable non-dimensional numbers is the Reynolds number based on the Taylor microscale

$$\mathrm{Re}_\lambda = \frac{v'\lambda}{\nu_t}, \qquad \lambda = \left(\frac{\sigma_{uu}^2}{\sigma_{\omega\omega}^2}\right)^{1/2}, \tag{28}$$

where ν_t is the eddy viscosity based on the Taylor microscale, λ, and $\vec{\omega} = \vec{\nabla} \times \vec{u}$ is vorticity in fluid. Muschinski [30] used another non-dimensional number, namely, the microstructure Knudsen number to characterize LES fluids.

It is convenient to express Re_λ in terms of the grid resolution and subfilter turbulent stress of the LES code. Recall that the mean vorticity variation is $\sigma^2_{\omega\omega} \propto \varepsilon/\nu_t \propto ||\tau^*_{ij}|| \cdot ||S^l_{ij}||/\nu_t$. If we also assume that λ is within the inertial interval of scales, where motions are almost isotropic, then the Smagorinsky–Lilly assumption gives $\nu_t \propto \Delta^2||S^l_{ij}||$. Thus, one can rewrite

$$\mathrm{Re}_\lambda \propto \frac{E\Delta}{\Delta^2||S^l_{ij}|| \cdot ||\tau^*_{ij}||^{1/2}} \propto \frac{H}{\Delta} \cdot \frac{E^{1/2}}{|u^g|} \cdot \left(\frac{E}{||\tau^*_{ij}||}\right)^{1/2}, \tag{29}$$

where we used $||S^l_{ij}|| \propto |u^g|/H$. Here, Δ is the grid resolution, E is the TKE, u^g is geostrophic velocity.

There is a number of assumptions behind Equation (29). Nevertheless, it highlights two factors determining Re_λ in LES. The first factor is the grid resolution, Δ. The relation, $\mathrm{Re} \propto \Delta^{-1}$, has been already discussed by Mason and Callen [52] and Muschinski [30]. The second factor is the ratio between the TKE and the subfilter turbulent stress. Latter two quantities are not independent in the LES code. Their ratio remains large only in the case of large spatial and temporal fluctuations of τ^*_{ij}. The ratio $E^{1/2}/|u^g|$ reflects the fact that the increase of the wind amplifies turbulent fluctuations in sheared flows.

Until Re is not very high ($\mathrm{Re} \approx 3 - 4 \cdot 10^4$ or $\mathrm{Re}_\lambda \approx 4 - 8 \cdot 10^2$ according to Wei and Willmarth [53]), turbulent statistics especially higher order statistics demonstrate considerable dependence on Re_λ. As the matter of fact, our interest is to obtain Re-independent statistics rather than to conduct truly infinite Re LES. Therefore the effect of the grid resolution and the turbulence closure will be considered below in comparison with experimental and observational data.

Sensitivity studies with respect to the grid resolution and the turbulence closure appear to be a popular subject (e.g., [20, 54–56]). Distinctive property of this study is that both the resolution and closure effects are considered from a common position.

3.2. EFFECT OF GRID RESOLUTION

Any physically meaningful LES code must demonstrate convergence of turbulence statistics with refinement of grid resolution. Figure 9 shows the convergence of the TKE profiles in PBLs. Indeed, the TKE profiles do converge. Moreover, even the coarsest LES run reproduces the TKE profile from the finest LES run in the PBL core ($0.2H$–$1H$). This fact is entirely in agreement with the Chapman's analysis and experimental findings by Wei and Willmarth [53]. It indicates that low order turbulent statistics become Re-independent at small Re_λ (large Δ in Equation (29)). The resolution of 10 grid points or so on the length scale H appears to be reasonable for the proper description of almost isotropic turbulence (see Figure 2) in the PBL core. This conclusion also gains an indirect support from many suc-

cessful coarse LES of convective boundary layers (e.g., [54, 57]). The convective turbulence is simply more isotropic.

Spectral analysis of PBL turbulence [8] reveals the well-developed inertial interval of scales. LES with the DMM, even the coarsest run, reproduce Kolmogorov's turbulence rather well (see Figure 6). This is expected since the DMM was optimized for it. Some explanation should be given to the steep spectral fall-off on the smallest resolved scales. Obviously, this fall-off is unphysical. Implicit filtering by the numerical schemes damps the smallest resolved scales [29, 58]. However, there is very little energy on the smallest scales. The DMM itself implicitly accounts for this damping in the optimization procedure. The accounting is so effective that the damping is practically compensated in the coarsest resolution run. Thus, it does not hamper overall LES results. The spectra also disclose another problem with simulations. The energy production interval of scales (spectral slope k^{-1}) is hardy resolved in domain as small as $4 \times 2.5 \times 2$ km (F.T.M Nieuwstadt, personal communication). Simulations in some larger domain are necessary. Analysis of atmospheric measurements suggests that a domain size between 15 and 30 km. would be more relevant for PBL simulations. In turn, this suggestion severely limits the LES resolution feasible at modern computers.

We are interested not only in the convergence as such but in the convergence toward measured data. Figure 9 seems to demonstrate failure of the LES technique to cope with the real world. Indeed, LES provide much less normalized TKE in the PBL core than it has been measured in the atmosphere and in laboratory experiments as well. Moreover, atmospheric and laboratory data, being very different in Re_λ, surface roughness etc., have better agreement with each other than with LES data. Mason and Brown LES [55] also showed such discrepancy. Contrary, Moeng and Sullivan LES [59] showed good agreement with data. Recently, it has been shown by Zilitinkevich and Esau [60] that there is better agreement between measurements and LES when the latter ones account for a strong temperature inversion. The inversion was prescribed in Moeng and Sullivan LES but not in Mason and Brown LES. The role of the capping inversion is not completely understood. Indeed, many studies dealing with data analysis do not consider the inversion strength as a key parameter at all (e.g., [40, 42, 61]). Other studies consider the inversion only in connection with turbulent properties of the upper part of PBL and entrainment processes (e.g., [57, 62]). The inversion can be considered as a rigid lid or a radiative surface. In any case, the inversion limits the largest size of turbulent eddies in PBLs. Surprisingly, it has larger effect on the turbulent surface stress than on the TKE so the ratio E/u_*^2 is increasing. This is in line with a 'top-down' turbulence theory. The theory was proposed by Hunt and Morrison [4] and Hunt and Carlotti [5] and gained some support from measurements by Högström *et al.* [63]. The author designed two LES runs to prove the critical importance of the largest eddies in PBLs. The PBL64-DMM-H500 run simulates the effect of a rigid lid in a shallow, 500 m., domain. The PBL64-DMM-CI run simulates the effect of a strong capping inversion, $\nabla_z \Theta = 5 \cdot 10^{-3}$ K m^{-1}. Profiles of the mean velocity and mean

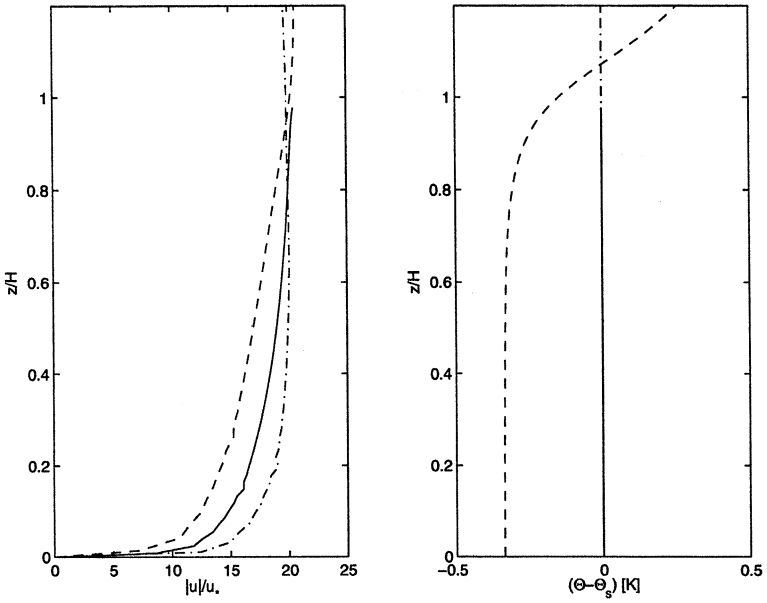

Figure 8. Profiles of the normalized mean velocity (a) and mean deviation of the potential temperature from its surface value Θ_S (b) at the steady state for the PBL64-DMM-H500 (solid line), PBL64-DMM-CI (dashed line) and PBL64-DMM (dashed-dotted line) runs.

potential temperature for these runs are shown in Figure 8. Figures 9 and 10 show that both runs reproduce atmospheric data better than LES runs in the deep domain. Sorbjan [57] published more detailed study of this effect in the convective PBL.

This analysis corroborates a widely spread view that the largest, therefore well resolved, turbulent eddies determine the PBL properties both in the PBL core and in the direct vicinity of the surface. Hence, the LES technique is not only a firmly grounded but also powerful prognostic technique. Particularly, the apparent failure of LES in PBLs has resulted in the discovery of a new important scaling parameter, namely, the imposed stability parameter, $N/|f|$, where N is the Brunt–Väisälä frequency of the free flow [60, 64]. Simulated and measured PBLs are similar only if they have approximately equal values of all scaling parameters. The scaling parameters are $|u^g|/(z_0|f|)$ and $N/|f|$ in the neutral case. Unfortunately, the imposed stability parameter has never appeared in available data. Probably, it was not measured even. It makes the LES verification vulnerable to a large systematic bias with respect to the set of the atmospheric measurements. Generally, LES better represent laboratory experiments, where the imposed stability is not defined.

The lower PBL constitutes of significantly anisotropic turbulence. The convergence of the TKE profiles increasingly deteriorates below $0.2H$ and down to the surface. It is a mere manifestation of scale restrictions in the surface layer. The size of isotropic eddies scales within this layer as κz, where $\kappa = 0.41$ is von Karman constant. The 2nd order finite difference schemes cannot resolve any

fluctuations on scales smaller than 2Δ. Therefore, the physical fluctuations below $z \approx 2\Delta/\kappa \approx 4\Delta$ are completely unresolved. At the first glance, it is reasonable to view turbulence at the lowermost layers in LES as a numerical artifact. However, the above conclusion does not bury the LES technique as such. Whether or not those fluctuations are artificial, they have to match the log-law boundary conditions. They have to match fully resolved large eddies in the PBL core too. So a more correct view of the surface layer turbulence would be as an imprint of large eddies with some artificial small details. Those small details do not harm much statistical properties of LES with the DMM. Figure 11a shows that the non-dimensional gradient of velocity is very close to its theoretical value $\Phi_m = 1$ even in the coarse resolution run. The spectra do not extend into the inertial interval of scales but they do resemble the energy producing interval of scales. Invariant PBL parameters such as a stress correlation coefficient $r_s = -\sigma_{uw}^2/(\sigma_{uu}\sigma_{ww})$ are also reproduced rather well (see Figure 12).

We have just seen that the normalized second order statistics are not sensitive to the LES resolution. There is, however, an increase of absolute values of the TKE with the resolution refinement. It is expectable since a so called subgrid-scale was not added here. TKE The higher order statistics are more sensitive to small scale fluctuations and therefore to Re_λ of the LES fluid. Figure 13 presents profiles of the vertical flux of the TKE, σ_{we}^3 (a), and the third order moment of the vertical velocity, σ_{www}^3 (b). These third order statistics are not reproduced with sufficient accuracy even in the finest run PBL128-DMM. Moreover, scale restrictions in the PBL64-DMM-H500 and PBL64-DMM-CI runs have little effect in this case. All runs consistently converge toward the PBL128-DMM profile. This convergence is not shown in Figure 13. Nevertheless, the detailed analysis of the third order statistics in LES shows that they do resemble the measured ones during transition periods in LES. We can speculate that atmospheric data was not obtained under proper steady state conditions. There is too large scatter in data and too little information about the PBL history, thus, it is not possible to design LES runs and to prove or to refute our suspicious about incomplete steady state of atmospheric data.

The TKE spectra in the surface layer have only energy production interval of scales. Only the PBL128-DMM run accounts for some portion of the inertial interval of scales. In spite of such a brutal violation of Smagorinsky–Lilly assumption, the DMM is still able to provide reasonable turbulent statistics and even spectral distribution of the TKE. This is due to instant optimization of the eddy viscosity, which balances the TKE at every time step. The mean profiles of the Smagorinsky constant in Figure 3 are consistent with the gradual decrease of the eddy viscosity in the surface layer and in coarser resolution runs.

3.3. EFFECT OF SUBGRID CLOSURE

The effect of the subgrid closure on LES results is more subtle than the effect of the grid resolution. The effect is mainly confined in critical layers like the surface layer

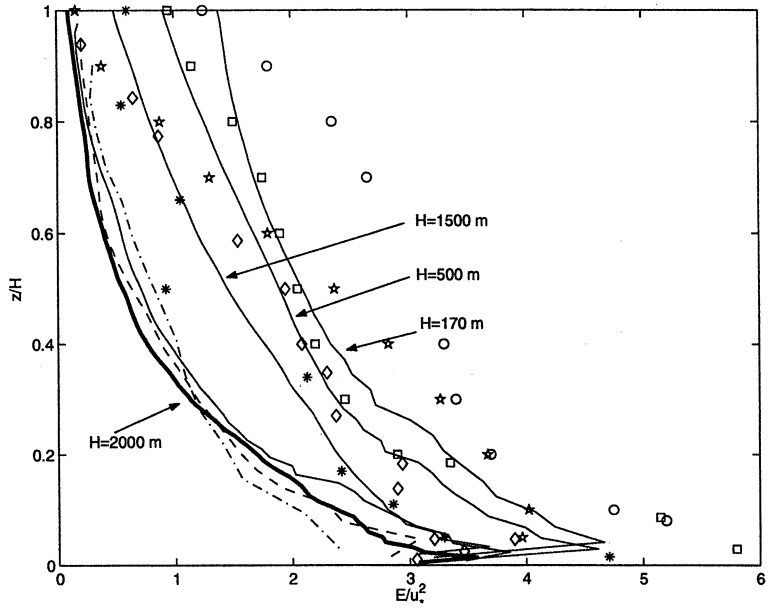

Figure 9. Profiles of the non-dimensional TKE, E/u_*^2, from LES with the DMM in the deep domain ($H = 2000$ m) at different resolutions: — run PBL128-DMM; — run PBL64-DMM; – – – run PBL32-DMM;– · – run PBL16-DMM. The additional solid curves show E/u_*^2 in shallow domain, the runs PBL80-DMM ($H = 1500$ m) and PBL64-DMM-H500 ($H = 500$ m), and in the inversion capped PBL, the run PBL64-DMM-CI ($H = 170$ m). The symbols are: $*$ PBL data from [41]; ○ PBL data from [40]; □ PBL data from [42]; ⋆ laboratory data from [39]; ◇ laboratory data from [38].

and the capping inversion. There is actually no reason to prefer the computationally expensive DMM to the traditional Smagorinsky closure in the case of (i) well resolved, (ii) steady-state, (iii) isotropic turbulent flow. Conditions (i)–(iii) are hard to satisfy in practical LES. Studies of heterogenous PBLs or coherent structures necessarily violate the condition (i). Studies of turbulence diurnal cycles or the inertial oscillation violate the condition (ii). Studies of the surface layer turbulence or stably stratified PBLs violate the condition (iii). Hence, it is generally unknown whether the LES with the TSM will provide reliable results or not. On the contrary, the DMM will always provide the best possible results under given set of physical assumptions (the Smagorinsky–Lilly eddy-viscosity assumption) and optimization methods (the least squared minimization).

To prove the above thesis, let us analyze the non-dimensional velocity gradient, Φ_m, in Figure 11 and the TKE spectra in Figure 7. The LES with the TSM1 ($C_s = 0.23$) strongly suppress the turbulent fluctuations. This is visible as $\Phi_m \gg 1$ and as a steep fall-off of the TKE spectra (Figure 7f). The PBL16-TSM1 run fails to reproduce turbulence at all. In this run, Re_λ drops below a critical $\mathrm{Re}_\lambda \approx 1$ (in definition by Equation (28)) in LES fluid. The resolution refinement simply makes the layer of overdamped turbulence more shallow in Figure 11c. Simultaneously,

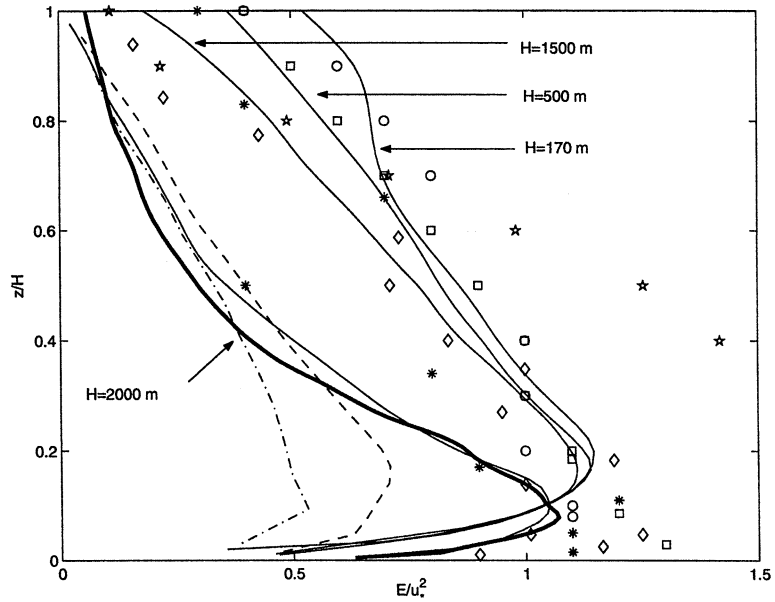

Figure 10. The same as in Figure 9, but for the non-dimensional vertical velocity variance, σ_{ww}^2/u_*^2

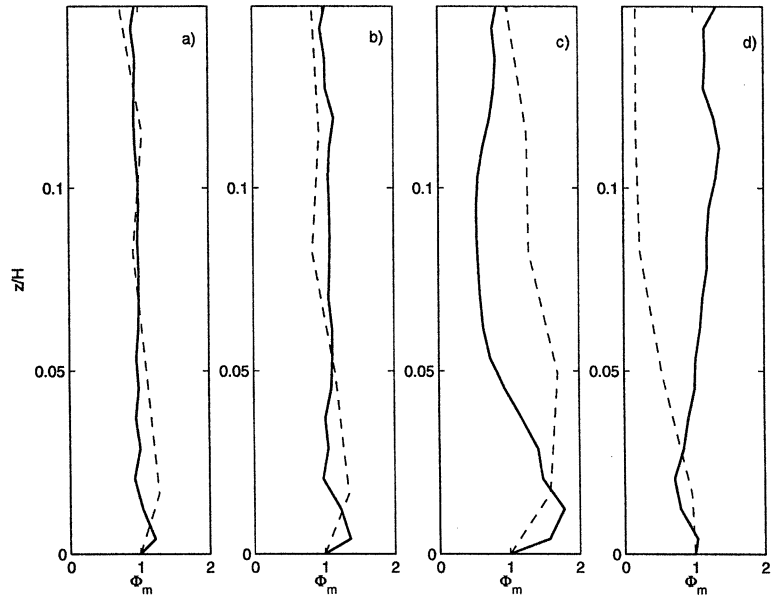

Figure 11. Profiles of non-dimensional velocity gradients, Φ_m, from the PBL128 (solid line) and PBL32 (dashed line) runs: (a) LES with the DMM; (b) LES with the DSM; (c) LES with the TSM1, $C_s = 0.23$; (d) LES with the TSM0, $C_s = 0.06$. The theory of neurally stratified boundary layers gives $\Phi_m = 1$.

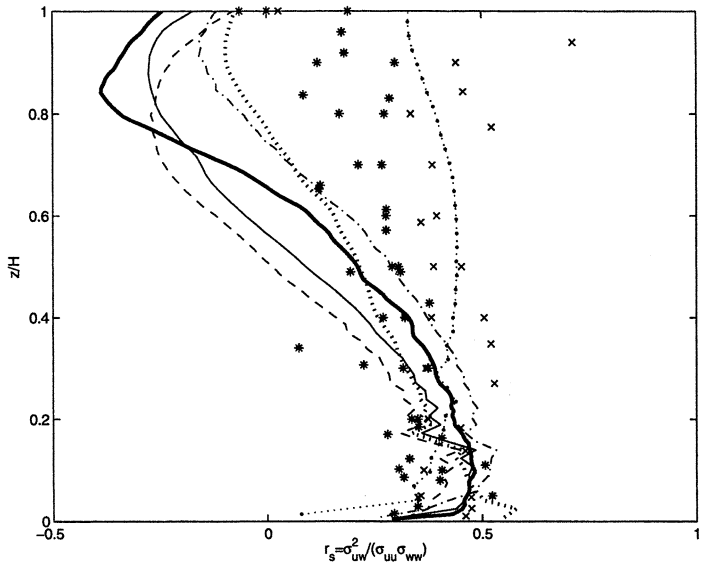

Figure 12. Profiles of the turbulent stress-velocity correlation coefficient, $r_s = -\sigma^2_{uw}/(\sigma_{uu}\sigma_{ww})$, from LES with different turbulence closures: — run PBL128-DMM; — run PBL64-DMM; – – – run PBL64-DSM;–·– run PBL64-TSM0; · · · run PBL64-TSM1; · · • · · • ·· run PBL64-DMM-CI. The symbols are: ∗ PBL data from [40, 42, 43]; × laboratory data from [38, 39, 41].

this refinement aggravates problems in that shallow layer, $\Phi_m^{128} > \Phi_m^{32} \gg 1$. This is entirely in agreement with Mason [19] findings. One possible solution is to reduce the eddy viscosity. The PBL32-TSM0 run have the same H/Δ but larger ratio $E/||\tau^*_{ij}||$. It shows the correct profile, $\Phi_m^{32} \approx 1$, in Figure 11d. However, the spectra now look ridiculous. Small scale fluctuation are overamplified and do not show any inertial or production intervals of scales. The resolution refinement does not improve the spectral behavior but disturbs Φ_m. Mason and co-authors [19, 22, 56] came up with similar conclusions. Thus, a careful tuning of C_s is needed to maintain reasonable level of the TKE and its spectral distribution for every resolution and at every PBL layer. That is exactly what the DMM and DSM do.

The LES with the DMM provide only slight improvement relative to the LES with the DSM (Figures 11 and 13). However, the DMM is more theoretically grounded. It is also less dependent on the eddy-viscosity assumption since about 15% of the subfilter turbulent stress is calculated explicitly in the Leonard term. C_s profiles in Figure 3 reflect this fact.

The DMM introduces some important improvements in the time evolution of PBLs too. All runs have been started from the laminar flow. Contrary to previous claims, all PBL64 runs have managed to develop comparable levels of the TKE from pure round-off errors. The turbulization process was, however, very different between LES with different subfilter closures. Figure 14 shows the evolution of the

Table I. Geometrical and physical parameters of LES runs.

Abbrev.	Grid	Closure	Re_λ	Run time [min]	Comments
PBL16-DMM	16^3	DMM	5.3	4	
PBL32-DMM	32^3	DMM	24.5	24	
PBL64-DMM	64^3	DMM	116.7	2070	
PBL128-DMM	128^3	DMM	346.4	11500	
PBL16-TSM0	16^3	TSM	8.3	1	
PBL32-TSM0	32^3	TSM	27.7	16	
PBL64-TSM0	64^3	TSM	130.0	1190	
PBL128-TSM0	128^3	TSM	309.0	5887	
PBL16-DSM	16^3	DSM	8.2	4	
PBL32-DSM	32^3	DSM	29.7	25	
PBL64-DSM	64^3	DSM	118.0	2464	
PBL128-DSM	128^3	DSM	394.7	12800	
PBL16-TSM1	16^3	TSM	0.4	< 1	critical $Re_\lambda \approx 1$
PBL32-TSM1	32^3	TSM	19.3	15	
PBL64-TSM1	64^3	TSM	127.2	1120	
PBL128-TSM1	128^3	TSM	430.6	5800	
PBL80-DMM	80^3	DMM	321.3	NA	domain $4 \times 2.5 \times 1.5$ km.
PBL40-DMM	40^3	DMM	60.0	NA	the 'standard test' run domain $4 \times 2.5 \times 1.5$ km.
PBL64-DMM-H500	64^3	DMM	207.8	2309	domain $1.5 \times 1.5 \times 0.5$ km.
PBL64-DMM-CI	64^3	DMM	175.8	5822	$\nabla_z \Theta = 0.005$ K m^{-1} domain $1 \times 1 \times 0.3$ km.

integral TKE. The PBL64-TSM1 run goes through a long period of the laminar flow. It needs an occasional large perturbation to overcome the suppressive eddy viscosity. The turbulence approaches the steady state only in $2tf$. The PBL64-TSM0 run turbulizes in $0.3tf$ and approaches the steady state in $0.5tf$. Moreover, the PBL64-TSM0 and PBL64-TSM1 runs develop an excess of the TKE (30%–50%) at the beginning of the process. The PBL64-DSM run turbulizes as fast as the PBL64-DMM run does. The turbulence approaches the steady state in $0.3tf$ in the PBL64-DSM run. The PBL64-DMM run shows a rapid and smooth transition to the steady state. The process takes about $0.25tf$.

Both the long laminar period and the excessive turbulence are very undesirable features of LES. They reduce our confidence to LES of any transitional processes in PBLs.

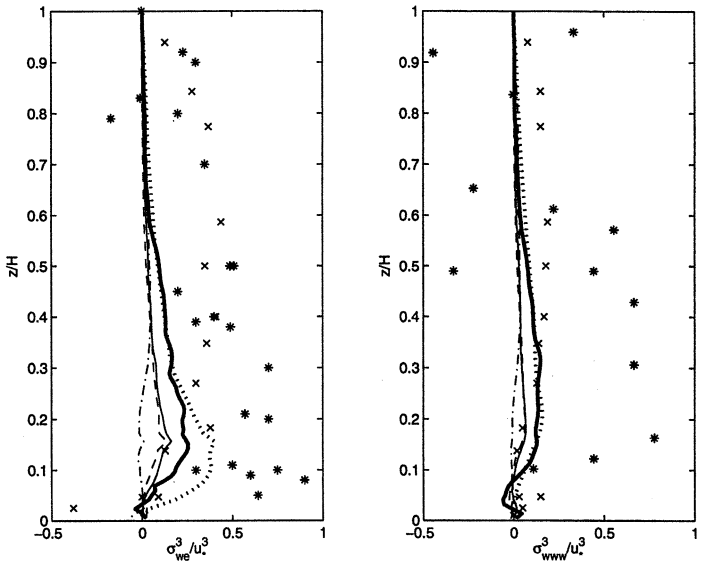

Figure 13. Profiles of the non-dimensional turbulent flux of the TKE (a) and the non-dimensional third order statistics of the vertical velocity fluctuations (b). The curves are as in Figure 12. The symbols are: $*$ PBL data from [43]; $\times$ laboratory data from [38].

LES fluid have smaller Re_λ than environmental fluids since the LES code represents only large scale motions and dissipates the TKE at relatively large grid scale. Respecting this resolution restrictions, the subfilter closure may vary Re_λ within a broad interval. Table I shows that the DMM runs ensure generally larger Re_λ than the TSM1 runs, especially at coarse resolution. Consequences are pleasant for the overall LES performance. Firstly, coarse LES still provide realistic turbulent statistics (see Figures 9 and 10). Snapshots of the TKE structure in Figure 16 discover intensive small scale fluctuations in the PBL128-DMM run but a smoother large scale fluctuations in the PBL128-TSM1 run. Due to these fluctuations, the LES with the DMM develops the logarithmic velocity profiles from the very first level while the LES with TSM develops a kind of artificial viscous sublayer comprising several first computational levels. Cai *et al.* [65] published more detailed analysis of velocity profiles in the LES with the TSM. Secondly, small scale details visible in Figure 16 lead to a more realistic partitioning of the TKE between Kolmogorov's turbulence and coherent structures. This partitioning was severely violated in earlier coarse simulations where simulated PBLs looked like a smooth low Re flows with a greatly exaggregated role of coherent structures like velocity streaks (e.g., [23]).

Summing up, the DMM maintains intensive velocity fluctuations on the smallest scales. These fluctuations are partially artificial due to practically zero energy dissipation in the majority of grid cells. Nevertheless, they help to simulate PBLs at higher Re_λ and maintain the correct TKE spectra. Figure 15 shows the direct

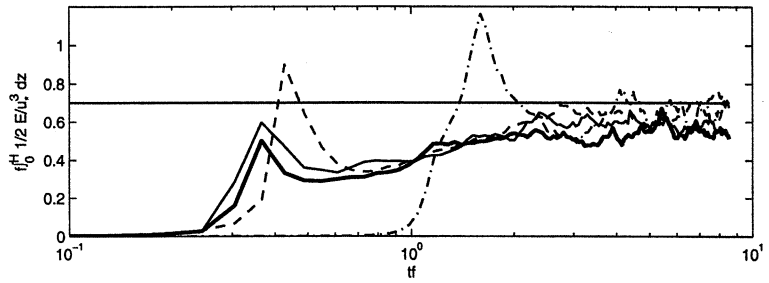

Figure 14. Time evolution of the integral non-dimensional TKE: — run PBL64-DMM; — run PBL64-DSM; – – – run PBL64-TSM0; –·– run PBL64-TSM1. The straight line shows the mean steady state level of the integral non-dimensional TKE in [17].

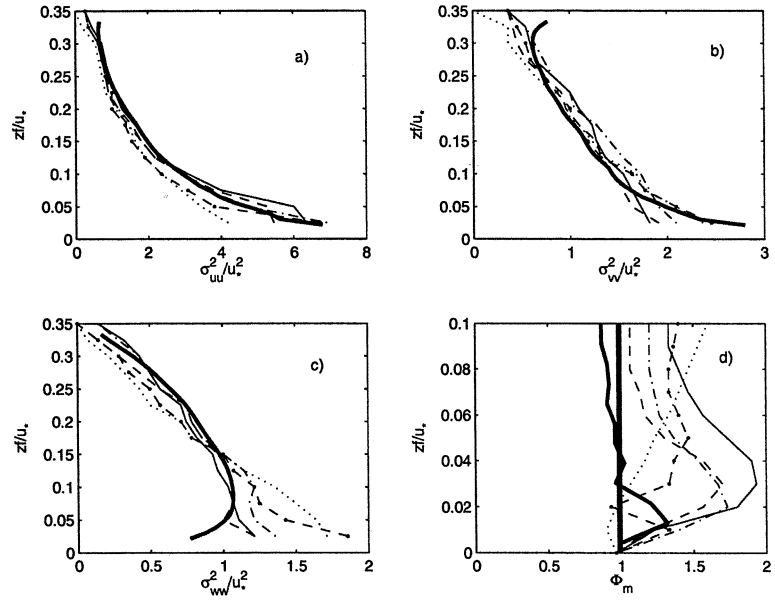

Figure 15. The 'standard test' of the PBL LES [17]. The curves are: — run PBL40-DMM; — Nieuwstadt's run; - - - - Andren/Moeng's run; –·– Mason/Brown's run; · · · · · Mason/Brown's backscatter run; — — — Schumann/Graf's run.

comparison between author's LES with the DMM (the PBL40-DMM run) and previous LES of other authors in a 'standard test' [17]. It is clearly seen that the second order statistics are comparable with other LES runs.

4. Conclusions

The study contains the description and the evaluation of the performance of the LES code LESNIC. The code incorporates the set of numerical methods, namely, the Runge–Kutta time scheme, the pressure correction scheme and the variable

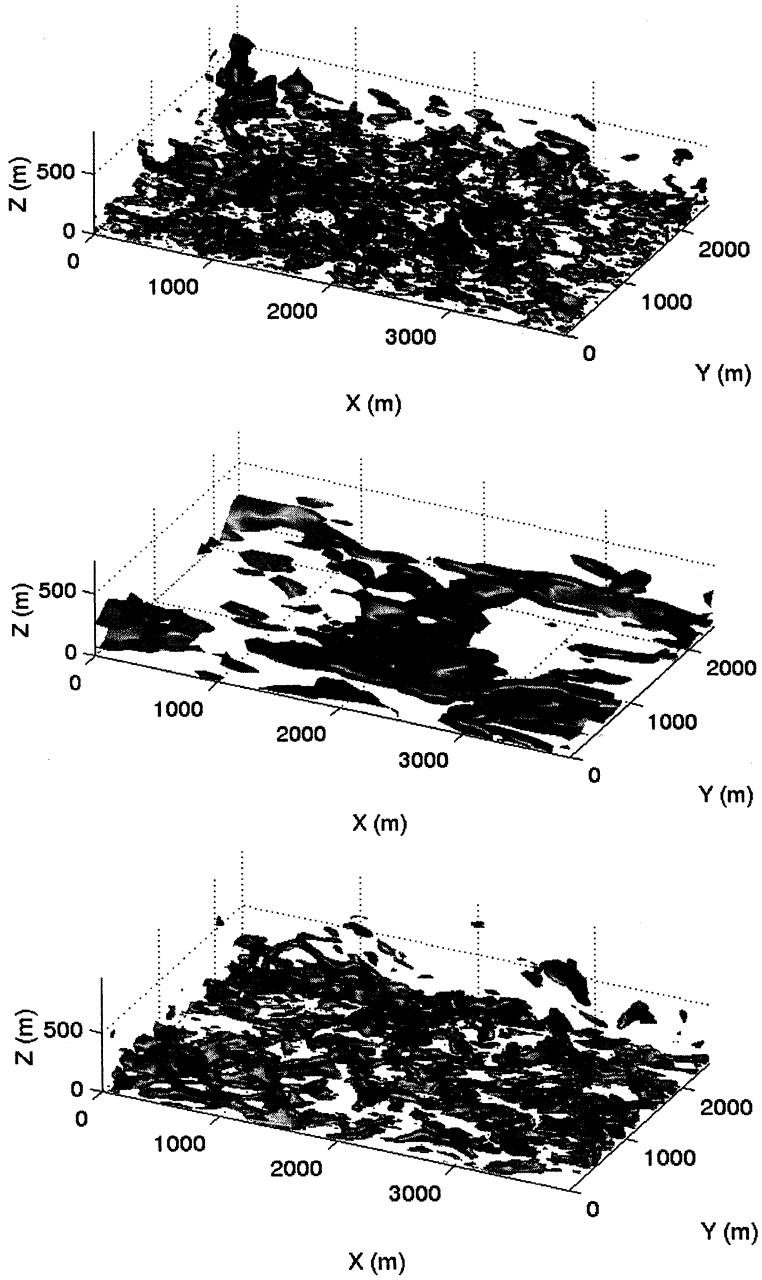

Figure 16. Snapshots of $1/2(u'^2 + v'^2 + w'^2)/u_*^2 = 5.5$ in the PBL128-DMM (upper panel), PBL32-DMM (middle panel) and PBL128-TSM1 (lower panel) runs.

time step, which are more common for engineering LES codes. These methods improve the computational performance of the code.

The main goal of this paper was to demonstrate consistency and robustness of the dynamic mixed turbulence closure in studies of the planetary boundary layer turbulence. Suitability of the DTCs for environmental high Re PBLs has been seriously questioned in previous publications. Although Porte-Agel *et al.* [21] and Zikanov *et al.* [32] have already used the LES with the DSM for PBL simulations, they did not publish convincing tests of their model performance against the simplest set of data.

The DMM has been introduced in a different way in this paper. The LESNIC performance was tested against laboratory and atmospheric data in neutral PBLs. The DMM is viewed as an optimization mathematical problem matching the eddy-viscosity assumption to the different degree of turbulence anisotropy in the PBL. Ultimate goal of the DMM is to ensure a balance between the local TKE and the local inertial TKE transport at the smallest scales. The balance is easy to ensure in the almost isotropic turbulence in the PBL core, where the inertial interval of scales is well resolved. Therefore, the DMM does not reveal any superiority with respect to more traditional turbulence closures in the PBL core. However, the DMM does reveal superiority in the surface layer and at coarse resolutions, where the inertial interval of scales is not resolved. In practical simulations, it is hardly possible to guarantee an adequate LES resolution throughout stratified PBLs. Thus, the DMM possesses some very desirable features for real world simulations. This study is not aimed to advocate one particular turbulence closure. The DMM is, perhaps, too computationally expensive. The LESNIC code with the DMM consumes twice as much time as the code with the TSM. An optimization method by Porte-Agel *et al.* [21] may reduce run time by 30–70%. Nevertheless, the turbulence statistics of the equal quality can be obtained using about 50% coarser grid in the LES with the DMM than in the LES with the TSM. It gives acceleration that more than compensate additional computational expenses.

The LESNIC code provides the Re-independent low-order turbulent statistics and the adequate TKE spectra at very coarse, $H/16$, resolution. Moreover, some statistics (the TKE and variations of the horizontal components of velocity) remain reasonable at $H/8$ resolution. It is in excellent agreement with Chapman's and Baggett *et al.* analysis. Reliable simulations of higher order statistics require something better resolution.

It has been shown that the effect of a rigid lid or a capping inversion must be represented in order to obtain LES comparable with laboratory and field measurements. Arbitrary choice of the domain size or the free flow stratification may be misleading. Ultimately, a careless choice of LES details may result in disregard of the LES technique as a suitable research tool.

Acknowledgements

This work has been started during the author's scholarship at the Department of Mechanical Engineering of Delft University of Technology. The author is grateful to Profs S.S. Zilitinkevich and F.T.M. Nieuwstadt, for useful suggestions and discussions. Technical advises by Drs V. Lykossov, B-J. Boersma, M. Tolstykh and L. Enger were useful for the code development. The work had a valuable support from the SIDA Project 'Non-local turbulent transport in weather prediction and air pollution modelling' – SRP-2000-036.

Appendix A

The simulations of the neutral PBLs are conducted in the domain $4000 \times 2500 \times 2000$ meters in x, y, z directions. The domain is deeper than in Andren *et al.* [17] simulations due to obvious influence of the top boundary conditions on the turbulent statistics in too shallow domain. It is demonstrated in this paper. The geostrophic wind is $u^g = \{5, 0\}$ m s^{-1}. Such a relatively slow wind alleviates the numerical restrictions on the model time step. All runs use the laminar flow as the initial state. All runs except PBL64-DMM-CI do not compute terms, which include potential temperature. In the PBL64-DMM-CI run, the temperature inversion was initially imposed throughout the whole domain. The surface roughness is $z_0 = 0.1$ m. The Coriolis parameter is $f = 10^{-4}$, which determines the latitude 45° North on Earth. All experiments run for 24 h of model time. These experiments enlisted in Table I.

The runs TSM0 have the Smagorinsky constant tuned down to $C_s = 0.06$. The runs TSM1 have the theoretical value of the Smagorinsky constant $C_s = 0.23$ [13]. The PBL40-DMM run is designed to reproduce exactly the 'standard test' [17].

The output of all runs is velocity fluctuations, $u_i'(x_j, t)$. The fluctuations are used to calculate turbulent statistics as $\sigma^2_{u_i u_j} = \overline{< u_i' u_j' >}$, $\sigma^3_{u_i u_j u_k} = \overline{< u_i' u_j' u_k' >}$ etc., where the superscript shows the order of the the statistics and the subscript shows variables involved in calculations. Here, the angular brackets denote averaging over the whole horizontal plain at every time step. The overbar denotes averaging over the time interval of $1tf$. The TKE spectra are calculated using one snapshot of the three-dimensional velocity field. The streamwise spectra are averaged in the normal, y, horizontal direction. The dissipation spectra are calculated using time series of horizontally averaged turbulent statistics. The time series were sampled every 10 min.

References

1. *Proceedings of the 15th Symposium on Boundary Layers and Turbulence*: 2002, 15–19 July, Wageningen, the Netherlands.
2. Raash, S. and Schröter M.: 2001, PALM — A large-eddy simulation model performing on massively parallel computers, *Meteorol. Z.* **10**, 363–372.

3. Coleman, G.N., Ferziger, J.H. and Spalart, P.R.: 1990, A numerical study of the turbulent Ekman layer, *J. Fluid Mech.* **213**, 313–348.
4. Hunt, J.C.R. and Morrison, J.F.: 2000, Eddy structure in turbulent boundary layers, *Mech. B–Fluids* **19**, 673–694.
5. Hunt, J.C.R. and Carlotti, P.: 2001, Statistical structure at the wall of the high Reynolds number turbulent boundary layer, *Flow, Turbulence Combustion* **65**, 453–475.
6. Kolmogorov, A.N.: 1941, The local structure of turbulence in incompressible viscous fluid for very large Reynolds numbers, *Dokl. Acad. Nauk. SSSR* **31**, 538–541.
7. Chapman, D. R.: 1978, Computational aerodynamics, development and outlook, *AIAA J.* **17**, 1293–1313.
8. Larson, S.: 1986, *Hot-Wire Measurements of Atmospheric Turbulence near the Ground*, Technical Report of RISOE National Laboratory, DK-4000 Roskilde, Denmark, **R-233**, 150 pp.
9. Chollet, J.P. and Lesieur, M.: 1981, Parameterization of small scales of three-dimensional isotropic turbulence utilizing spectral closures, *J. Atmos. Sci.* **38**, 2747–2757.
10. Metais, O. and Lesieur, M.: 1992, Spectral large-eddy simulations of isotropic and stably-stratified turbulence, *J. Fluid. Mech.* **239**, 157–194.
11. Piomelli, U.: 1999, Large-eddy simulation: achievements and challenges, *Progr. Aerospace Sci.* **35**, 335–362.
12. Germano, M., Piomelli, U., Moin, P. and Cabot, W.: 1991, A dynamic subgrid-scale eddy-viscosity model, *Phys. Fluids A* **5**, 2946–2968.
13. Lilly, D.K.: 1966, On the instability of Ekman boundary layer, *J. Atmos. Sci.* **2**, 481–494.
14. Smagorinsky, J.: 1963, General circulation experiments with the primitive equations, *Mon. Wea. Rev.* **91**, 99–164.
15. Zang, Y., Street, R.L. and Koseff, J.R.: 1993, A dynamic mixed subgrid-scale model and its application to turbulent recirculating flow, *Phys. Fluids* **5**, 3186–3196.
16. Baggett, J.S., Jimenez, J. and Kravchenko, A.G.: 1997, Resolution requirements in large-eddy simulations of shear flows, In: *Annual Res. Briefs*, Center for Turbulence Research, Stanford University, CA, pp. 51–66.
17. Andren, A., Brown, A.R., Graf, J., Mason, P.J., Moeng, C-H., Nieuwstadt, F.T.N. and Schumann, U.: 1994, Large-eddy simulation of a neutrally stratified layer: A comparison of four computer codes, *Quart. J. Roy. Meteorol. Soc.* **120**, 1457–1484.
18. Kosovic, B.: 1997, Subgrid-scale modelling for the large-eddy simulation of high-Reynolds-number boundary layers, *J. Fluid Mech.* **336**, 151–182.
19. Mason, P.J.: 1994, Large-eddy simulation: A critical review of the technique, *Quart. J. Roy. Meteorol. Soc.* **120**, 1–26.
20. Moeng, C.-H., Cotton, W.R., Bretherton, C., Chlond, A., Khairoutdinov, M., Krueger, S., Lewellen, W.S., MacVean, M.K., Pasquier, J.R.M., Rand, H.A., Siebesma, A.P., Stevens, B. and Sykes, R.I.: 1996, Simulation of a stratocumulus-topped planetary boundary layer: Intercomparison among different numerical codes, *Bull. Amer. Meteorol. Soc.* **77**, 261–278.
21. Porte-Agel, F., Meneveau, C. and Parlange, M.B.: 2000, A scale-dependent dynamic model for large-eddy simulation: Application to a neutral atmospheric boundary layer, *J. Fluid Mech.* **415**, 262–284.
22. Mason, P.J. and Thomson, D.J.: 1992, Stochastic backscatter in large eddy simulations of boundary layers, *J. Fluid Mech.* **242**, 51–78.
23. Sullivan, P.P., McWilliams, J.C. and Moeng, C.-H.: 1994, A subgrid scale model for large eddy simulation of planetary boundary layer flows, *Boundary-Layer Meteorol.* **71**, 247–276.
24. Vreman, B., Geurts, B. and Kuerten, H.: 1994, On the formulation of the dynamic mixed subgrid-scale model, *Phys. Fluids* **6**, 4057–4059.
25. Vreman, B., Geurts, B. and Kuerten, H.: 1997, Large-eddy simulation of the turbulent mixing layer, *J. Fluid Mech.* **339**, 357–390.

26. Kraichnan, R.H.: 1976, Eddy viscosity in two and three dimensions, *J. Atmos. Sci.* **33**, 1521–1536.
27. Leslie, D.C. and Quarini, G.L.: 1979, The application of turbulence theory to the formulation of subgrid modelling procedures, *J. Fluid Mech.* **91**, 65–91.
28. Tong, C., Wyngaard, J.C. and Brasseur, J.G.: 1999, Experimental study of the subgrid-scale stresses in the atmospheric surface layer, *J. Atmos. Sci.* **56**, 2277–2292.
29. Kravchenko, A.G. and Moin, P.: 1997, On the effect of numerical errors in large eddy simulations of turbulent flows, *J. Comput. Phys.* **131**, 310–322.
30. Muschinski, A.: 1996, A similarity theory of locally homogeneous and isotropic turbulence generated by a Smagorinsky-type LES, *J. Fluid Mech.* **325**, 239–260.
31. Zikanov, O., Slinn, D.N. and Dhanak, M.R.: 2002, Turbulent convection driven by surface cooling in shallow water, *J. Fluid Mech.* **464**, 81–111.
32. Zikanov, O., Slinn, D.N. and Dhanak, M.R.: 2003, Large eddy simulations of the wind-induced turbulent Ekman layer, *J. Fluid Mech.* **495**, 343–368.
33. Sullivan, P.P., Horst, Th.W., Lenschow, D.H., Moeng, C.-H. and Weil, J.C.: 2003, Structure of subfilter-scale fluxes in the atmospheric surface layer with application to large-eddy simulation modeling, *J. Fluid Mech.* **482**, 101–139.
34. Ghosal, S., Lund, T.S., Moin, P. and Akselvoll, K.: 1995, A dynamic localization model for large-eddy simulation of turbulent flows, *J. Fluid Mech.* **286**, 229–255.
35. Germano, M.: 1992, Turbulence: the filtering approach, *J. Fluid Mech.* **238**, 325–336.
36. Salvetti, M.V. and Banerjee, S.: 1995, A priori tests of a new dynamic subgrid-scale model for finite difference large eddy simulations, *Phys. Fluids* **7**, 2831–2847.
37. Salvetti, M.V. and Beux, F.: 1998, The effect of the numerical scheme on the subgrid scale term in large-eddy simulation, *Phys. Fluids* **10**, 3020–3022.
38. Andreopoulos, J. and Bradshaw, P.: 1981, Measurements of turbulence structure in the boundary layer on a rough surface, *Boundary-Layer Meteorol.* **20**, 201–213.
39. Krogstad, P.A., Antonia, R.A. and Browne, L.W.B.: 1992, Comparison between rough- and smooth-wall turbulent boundary layers, *J. Fluid Mech.* **245**, 599–617.
40. Grant, A.L.M.: 1986, Observations of boundary layer structure made during the 1981 KONTUR experiment, *Quart. J. Roy. Meteorol. Soc.* **112**, 825–841.
41. Pennell, W.T. and LeMone, M.A.: 1974, An experimental study of turbulence structure in the fair-weather trade wind boundary layer, *J. Atmos. Sci.* **31**, 1308–1323.
42. Tjernström, M. and Smedman, A.-S.: 1993, The vertical structure of the coastal marine atmospheric boundary layer, *J. Geophys. Res.* **98**(C3), 4809–4826.
43. Brost, R.A., Wyngaard, J.C. and Lenshow, D.H.: 1982, Marine stratocumulus layers. Part II: Turbulence budgets, *J. Atmos. Sci.* **39**, 818–836.
44. Liu, S., Meneveau, C. and Katz, J.: 1994, On the properties of similarity subgrid-scale models as deduced from measurements in a turbulent jet, *J. Fluid Mech.* **275**, 83–119.
45. Kondo, J., Kanechika, O. and Yasuda, N.: 1978, Heat and momentum transfer under strong stability in the atmospheric surface layer, *J. Atmos. Sci.* **35**, 1012–1021.
46. Morinishi, Y., Lund, T.S., Vasilyev, O.V., and Moin, P.: 1998, Fully conservative higher order finite difference schemes for incompressible flow, *J. Comput. Phys.* **143**, 90–124.
47. Sagaut, P. and Grohens, R.: 1999, Discrete filters for large eddy simulation, *Int. J. Num. Mech. Fluids* **31**, 1195–1220.
48. Jameson, A., Schmidt, W. and Turkel, E.: 1981, Numerical simulation of the Euler equations by finite 77 volume methods using Runge–Kutta time stepping schemes, *AIAA Paper* **81**, 1259.
49. Kim, J. and Moin, P.: 1985, Application of fractional step method to incompressible Navier–Stokes equations, *J. Comput. Phys.* **59**, 308–323.
50. Armfield, S. and Street, R.: 1999, The fractional step method for the Navier-Stokes equations on staggered grids: The accuracy of three variations, *J. Comput. Phys.* **153**, 660–665.
51. Lesieur, M.: 1997, *Turbulence in Fluids*, Kluwer Academic Publishers, Dordrecht, 532 pp.

52. Mason, P.J. and Callen, N.S.: 1986, On the magnitude of the subgrid-scale eddy coefficient in large-eddy simulations of turbulent channel flow, *J. Fluid Mech.* **162**, 439–462.
53. Wei, T. and Willmarth, W.W.: 1989, Reynolds-number effects on the structure of a turbulent channel flow, *J. Fluid Mech.* **204**, 57–95.
54. Agee, E. and Gluhovsky, A.: 1999, LES model sensitivities to domains, grids, and large-eddy timescales, *J. Atmos. Sci.* **56**, 599–604.
55. Mason, P.J. and Brown, A.R.: 1994, The sensitivity of large-eddy simulations of turbulent shear flow to subgrid models, *Boundary-Layer Meteorol.* **70**, 133–150.
56. Mason, P.J. and Brown, A.R.: 1999, On subgrid models and filter operations in large-eddy simulations, *J. Atmos. Sci.* **56**, 2101–2114.
57. Sorbjan, Z.: 1996, Numerical study of penetrative and 'solid lid' non-penetrative convective boundary layers, *J. Atmos. Sci.* **53**, 101–112.
58. Schmidt, H. and Schumann, U.: 1989, Coherent structure of the convective boundary layer derived from large-eddy simulations, *J. Fluid Mech.* **200**, 511–562.
59. Moeng, C.-H. and Sullivan, P.: 1994, A comparison of shear- and buoyancy-driven planetary boundary layer flows, *J. Atmos. Sci.* **51**, 999–1022.
60. Zilitinkevich, S.S. and Esau, I.N.: 2002, On integral measures of the neutral barotropic planetary boundary layer, *Boundary-Layer Meteorol.* **104,** 371–379.
61. Hess, G.D. and Garratt, J.R.: 2002, Evaluating models of the neutral, barotropic planetary boundary layer using integral measures: Part I. Overview, *Boundary-Layer Meteorol.* **104**, 333–358.
62. Otte, M.J. and Wyngaard, J.C.: 2001, Stably stratified interfacial-layer turbulence from large eddy simulations, *J. Atmos. Sci.* **58**, 3424–3442.
63. Högström, U., Hunt, J.C.R. and Smedman, A.-S.: 2003, Theory and measurements for turbulence spectra and variances in the atmospheric neutral surface layer, *Boundary-Layer Meteorol.* **103**, 101–124.
64. Zilitinkevich, S.S. and Esau, I.N.: 2003, The effect of baroclinicity on the depth of neutral and stable planetary boundary layers, *Quart. J. Roy. Meteorol. Soc.*, to appear.
65. Cai, X., Steyn, D.G. and Gartshore, I.S.: 1995, Resolved scale turbulence in the atmospheric surface layer from a large eddy simulation, *Boundary-Layer Meteorol.* **75**, 301–314.